



Nanoscale

**A First Glance into Mixed Phosphine-Stibine Moieties as  
Protecting Ligands for Gold Clusters**

Journal:	<i>Nanoscale</i>
Manuscript ID	NR-ART-10-2022-005497.R1
Article Type:	Paper
Date Submitted by the Author:	23-Mar-2023
Complete List of Authors:	Singh, Kundan; Southern Methodist University, Chemistry Bhattacharyya, Ayan ; Southern Methodist University Havenridge, Shana; Kansas State University, Chemistry Ghabin, Mohamed; Southern Methodist University Ausmann, Hagan; Southern Methodist University Siegler, Maxime; Johns Hopkins University, Chemistry Aikens, Christine; Kansas State University, Chemistry Das, Anindita; Southern Methodist University, Chemistry;

SCHOLARONE™  
Manuscripts

# A First Glance into Mixed Phosphine-Stibine Moieties as Protecting Ligands for Gold Clusters

Kundan K. Singh<sup>a†</sup>, Ayan Bhattacharyya<sup>a†</sup>, Shana Havenridge<sup>b</sup>, Mohamed Ghabin<sup>a</sup>, Hagan Ausmann<sup>a</sup>, Maxime A. Siegler<sup>c</sup>, Christine M. Aikens<sup>b\*</sup> & Anindita Das<sup>a\*</sup>

a) Department of Chemistry, Southern Methodist University, Dallas, Texas 75275, United States

b) Department of Chemistry, Kansas State University, Manhattan, Kansas 66506, United States

c) Department of Chemistry, Johns Hopkins University, Baltimore, Maryland 21218, United States

† : These authors have contributed equally.

## Abstract

Atomically precise gold clusters have attracted considerable research interest as their tunable structure-property relationships have resulted in widespread applications, from sensing and biomedicine to energetic materials and catalysis. In this article, the synthesis and optical properties of a novel  $[\text{Au}_6(\text{SbP}_3)_2][\text{PF}_6]_2$  cluster are reported. Despite the lack of spherical symmetry in the core, the cluster shows exceptional thermal and chemical stability. Detailed structural attributes and optical properties are evaluated experimentally and theoretically. This, to the best of our knowledge, is the first report of a gold cluster protected via synergistic multidentate coordination of stibine (Sb) and phosphine moieties (P). To further show that the latter moieties give a set of unique properties that differs from monodentate phosphine-protected  $[\text{Au}_6(\text{PPh}_3)_6]^{2+}$ , geometric structure, electronic structure, and optical properties are analyzed theoretically. In addition, this report also demonstrates the critical role of overall-ligand architecture in stabilizing mixed ligand-protected gold clusters.

## Introduction

Metal clusters, containing tens to hundreds of metal atoms and exhibiting strong metal-metal bonds, show unique quantum confinement effects and are generally considered a bridge between small molecules and bulk-materials. In recent years, ligand-protected gold clusters have attracted significant interest owing to their unique geometric structures and physicochemical properties which make these clusters suitable for a wide range of applications including catalysis, sensing, luminescence, and biomedicine.<sup>1,2</sup> Thiolate-, alkyne-, and phosphine-protected clusters, in particular, have dominated this realm of gold-cluster chemistry,<sup>3-10</sup> although heavier thiolate-analogues such as selenolates have also been explored to synthesize stable gold clusters.<sup>11</sup> On the other hand, heavier phosphine-analogues such as stibines are severely underexplored and have only recently garnered interest as potential ligands to stabilize gold clusters. In 2018, Leong *et al.*, reported the first stibine-protected gold cluster viz.  $[\text{Au}_{13}(\text{SbPh}_3)_8\text{Cl}_4]^+$ .<sup>12</sup> Very recently, Das *et al.*, reported the first mixed stibine-thiolate gold cluster formulated as  $\text{Au}_{18}(\text{S-Adm})_8(\text{SbPh}_3)_4\text{Br}_2$  (S-Adm=1-adamantanethiolate).<sup>13</sup> These two are the only reports of stibine-protected gold clusters to date. The underutilization of stibines as ligands is typically ascribed to their weaker coordinating ability from the diffuse donor orbitals.<sup>14,15</sup> However, it has been experimentally observed that the *mixed stibine-thiolate*-protected  $\text{Au}_{18}(\text{S-Adm})_8(\text{SbPh}_3)_4\text{Br}_2$  cluster exhibits enhanced stability compared to the *only-stibine*-protected  $[\text{Au}_{13}(\text{SbPh}_3)_8\text{Cl}_4]^+$  cluster.<sup>13</sup> This opens up the possibility that suitable multidentate ligand design involving stibines alongside strongly coordinating groups such as thiolates or phosphines, will lead to synergistic coordination modes, yielding robust clusters with unique structural attributes and optical

properties. It is worthy to note that such multidentate ligand platforms consisting of pyridyl phosphines and tetradentate phosphines have been successfully used to enhance the stability of phosphine-based Au clusters in previous studies.<sup>16,17</sup>

In this work, we synthesize and illustrate properties of a Au<sub>6</sub> cluster stabilized by a multidentate ligand containing one stibine (Sb) and three phosphine (P) moieties, in which the Au<sub>6</sub> core can be envisioned as comprising of two Au<sub>4</sub> tetrahedra which assemble together by sharing a common Au<sub>2</sub> edge (highlighted in green in **Fig. 1**). This, to the best of our knowledge, is the first report where a ligand containing both stibine and phosphine coordinating sites has been utilized as a protecting group for gold cluster synthesis. It is worthwhile to note that bidentate diphosphine ligands have been previously used to synthesize Au<sub>6</sub> clusters exhibiting “core+exo” structures comprising of a Au<sub>4</sub> tetrahedral core and 2 exo Au atoms, in sharp contrast to the edge-sharing bitetrahedral Au<sub>6</sub> core in the newly synthesized [Au<sub>6</sub>(SbP<sub>3</sub>)<sub>2</sub>][PF<sub>6</sub>]<sub>2</sub> cluster.<sup>18,19</sup> On the other hand, a similar bitetrahedral Au<sub>6</sub> core was observed only in the case of monodentate phosphine-protected Au<sub>6</sub> clusters.<sup>20-24</sup> Comparison of our results with [Au<sub>6</sub>(PPh<sub>3</sub>)<sub>6</sub>]<sup>2+</sup> re-affirmed the role of ligand architecture in stabilizing these cluster-geometries with multidentate ligands.<sup>20,21</sup> The role of ligand architecture was further illustrated using another mixed stibine-phosphine ligand containing one stibine (Sb) and two phosphine (P) moieties, ((phenylstibinediyl)bis(2,1-phenylene))bis(diphenylphosphine), abbreviated as SbP<sub>2</sub>.<sup>15,25</sup> It was observed that while cluster synthesis with SbP<sub>3</sub> results in a robust Au<sub>6</sub> cluster, analogous synthetic efforts with SbP<sub>2</sub> resulted in unstable clusters under similar experimental conditions. Thus, our report not only highlights the necessity of synergistic interactions of Sb and P moieties but also sheds light on the importance of overall-ligand architecture to achieve stable gold clusters.

## Experimental Section

**Materials:** All starting materials are of reagent grade or better. These were obtained from commercial sources (TCI, Sigma-Aldrich etc) and used without further purification.

**Thermal Stability:** A solution of [Au<sub>6</sub>(SbP<sub>3</sub>)<sub>2</sub>][PF<sub>6</sub>]<sub>2</sub> was prepared by dissolving 1 mg cluster in 2 mL ethanol. 500 μL of this stock solution was taken in a 2-sided quartz cuvette and diluted to 2 mL. This diluted solution was kept at 70°C and monitored via UV-vis absorption spectroscopy every 1 hour for 16 hours in total.

**Chemical Stability in presence of Glutathione:** The [Au<sub>13</sub>(SbPh<sub>3</sub>)<sub>8</sub>Cl<sub>4</sub>]<sup>+</sup> and [Au<sub>11</sub>(PPh<sub>3</sub>)<sub>8</sub>Cl<sub>2</sub>]<sup>+</sup> clusters were synthesized using previously reported literature protocols.<sup>10,12,26</sup> 3-4 mg of each cluster was dissolved in 4 mL dichloromethane (DCM). To each of them, an excess glutathione (25 eq with respect to the cluster) dissolved in 4 mL DI-water is added. Formation of two distinct layers is observed within 2 minutes. Then these mixtures are stirred vigorously for variable time-periods at 45°C.

## Computational Details

All calculations were completed using the Amsterdam Modeling Suite (AMS) 2021.1 package.<sup>27</sup> The initial unrefined crystal structure was used as an input structure for all calculations, which can be

described as a single monomer isolated from the packed crystal structure. Scalar relativistic effects were included by utilizing the zeroth-order regular approximation (ZORA).<sup>28,29</sup> All calculations were completed at the BP86-D3/DZP level of theory, where BP86 is a generalized gradient approximation (GGA) exchange-correlation functional,<sup>30,31</sup> -D3 refers to the dispersion effects added to the exchange-correlation functional via the Grimme3 model,<sup>32</sup> and a double-zeta polarized (DZP) basis set is used.<sup>33</sup> The theoretical absorption spectrum was calculated with linear response time-dependent density-functional theory plus tight binding (TDDFT+TB)<sup>34</sup> where the vertical excitation energies were convolved into the optical absorption spectrum with a gaussian fit with a full width half maximum (FWHM) of 30 nm (for plots shown in wavelength) or 0.20 eV (for plots shown in eV). The structure was optimized in the gas phase and the gradient convergence criteria was tightened to  $1 \times 10^{-3}$  Hartree for geometric accuracy. All calculations had a tightened SCF convergence requirement of  $1 \times 10^{-8}$ . Due to the locality of the GGA functional, as well as charge transfer character from the molecular orbital transitions, additional results are calculated with simplified time-dependent density-functional theory (sTDDFT)<sup>35</sup> with a Yukawa long-range separated hybrid functional with a gamma value of 0.75 on the optimized BP86-D3/DZP  $S_0$  state.<sup>36</sup> For the circular dichroism (CD) spectrum, the isolated  $Au_6^{2+}$  core was optimized at the BP86-D3/DZP level of theory in addition to the full cluster.

## Results and Discussion

The synthesis of the multidentate  $SbP_3$  ligand has been carried out with slight modifications of reported protocols,<sup>14,15,25</sup> and is described in detail in the ESI<sup>†</sup> (**S1.1** and **Fig. S1, S2**). The synthesis of the  $[Au_6(SbP_3)_2]^{2+}$  gold cluster is also discussed in detail under **S1.2** in the ESI<sup>†</sup>. Briefly, chloro(dimethylsulfide)gold(I) was reacted with  $SbP_3$  ligand in 1:1 ratio in dichloromethane (DCM), followed by the addition of ethanolic solution of  $NaBH_4$  at room temperature (25 °C) to synthesize the  $[Au_6(SbP_3)_2]^{2+}$  cluster. Counter ion exchange was achieved by a metathesis reaction using  $NaPF_6$  salt and orange-coloured single crystals were obtained by slow vapour diffusion of pentane into a DCM solution of  $[Au_6(SbP_3)_2]^{2+}$  at 4°C. The structure of the ligand  $SbP_3$  and the crystal structure of  $[Au_6(SbP_3)_2]^{2+}$  are shown in **Fig. 1**. The crystal structure of  $[Au_6(SbP_3)_2]^{2+}$  is best described in the triclinic space group  $P\bar{1}$ , with six gold atoms, two  $SbP_3$  ligands, and two  $PF_6^-$  ions (**Fig. 1(B)**).  $[Au_6(SbP_3)_2]^{2+}$  has a  $Au_6$  core composed of two edge-sharing tetrahedra (**Fig. 1(C)**), protected by two  $SbP_3$  ligands via multidentate coordination, where each Au atom bonds with one Sb atom and one P atom.

Electrospray ionization mass spectrometry (ESI-MS) was performed to confirm the mass of the  $[Au_6(SbP_3)_2][PF_6]_2$  cluster. A clean +2 peak at  $m/z$  of 1496.06 was observed in the positive mode, consistent with the cationic cluster formula of  $[Au_6(SbP_3)_2]^{2+}$  (**Fig. 2**). In addition, NMR studies were carried out to investigate the binding of the surface ligands of the  $[Au_6(SbP_3)_2][PF_6]_2$  cluster (**Fig. S2** and **S4**). A downfield shift of ca. 12 ppm in the phosphorous signal upon cluster formation indicates the presence of Au- $SbP_3$  ligand interactions, in turn, confirming the presence of  $SbP_3$  ligands on the cluster surface. In addition, the characteristic UV-vis bands of the cluster were centered around 368 nm and 462 nm (**Fig. S3**).

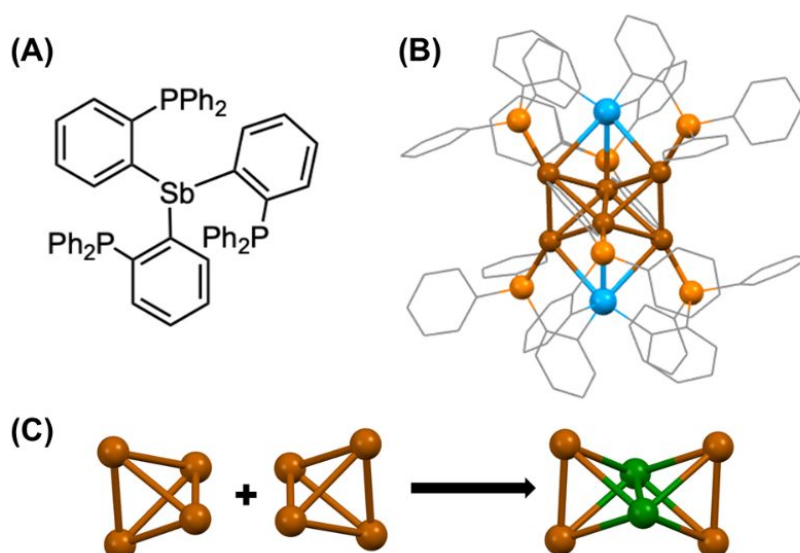


**Fig. 1** (A) Chemical structure of the mixed phosphine-stibine ligand ( $\text{SbP}_3$ ); (B) Total structure of  $[\text{Au}_6(\text{SbP}_3)_2]^{2+}$  cluster; (C) Structure of the  $\text{Au}_6$  core comprised of two  $\text{Au}_4$  tetrahedra which assemble together by sharing a common  $\text{Au}_2$  edge (highlighted in green). (Colour labels: brown/green = Au; orange = P; blue = Sb, grey = C; H atoms are not shown for clarity).

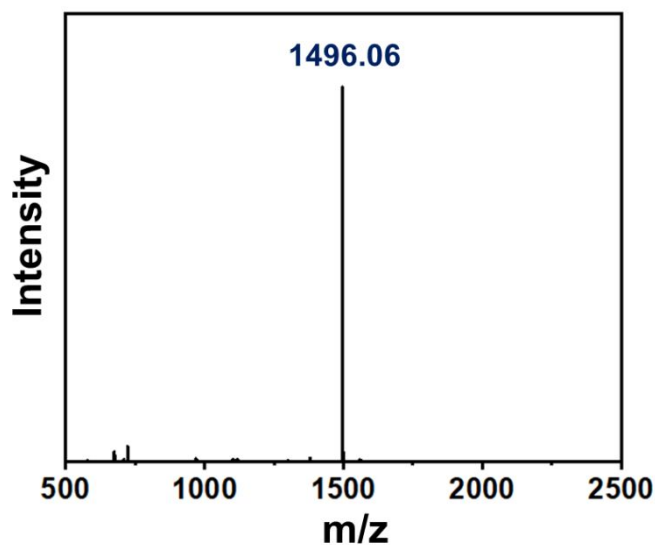


**Fig. 2** ESI-MS spectrum (positive mode) of the  $[\text{Au}_6(\text{SbP}_3)_2][\text{PF}_6]_2$  cluster. The peak at 1496.06 corresponds to  $m/z$  ( $z=2$ ) of intact cationic  $[\text{Au}_6(\text{SbP}_3)_2]^{2+}$  cluster (calculated  $m/z = 1496.05$ ).

Magic clusters, i.e. clusters that have fully filled superatomic orbitals, analogous to those of a noble gas, show high stability from the energetics between the spherically symmetric superatomic orbitals.<sup>37,38</sup> Both  $[\text{Au}_{13}(\text{SbPh}_3)_8\text{Cl}_4]^+$  and  $\text{Au}_{18}(\text{S-Adm})_8(\text{SbPh}_3)_4\text{Br}_2$  are examples of this with a superatomic electron count of 8 that yields a  $\text{S}^2\text{P}^6$  configuration.<sup>12,13</sup> Unlike these clusters, however,  $[\text{Au}_6(\text{SbP}_3)_2]^{2+}$  has a superatomic electron count of 4, corresponding to a  $\text{S}^2\text{P}^2$  configuration. As the P orbitals are not fully filled,

the cluster is less spherically symmetric and more prolate. Because of this, the cluster follows the ellipsoidal Clemenger-Nilsson shell model rather than the spherical shell (or superatomic) model.<sup>39</sup>  $[\text{Au}_6(\text{PPh}_3)_2]^{2+}$ , the monodentate phosphine-protected species, also has a superatomic electron count of 4 resulting in a more prolate geometry. Herein, to understand the exact role of ligands in dictating the core geometric and electronic structure, we performed calculations on monodentate phosphine-protected  $[\text{Au}_6(\text{PPh}_3)_6]^{2+}$  clusters<sup>20,21</sup> in addition to the mixed phosphine-stibine protected  $[\text{Au}_6(\text{SbP}_3)_2]^{2+}$ .

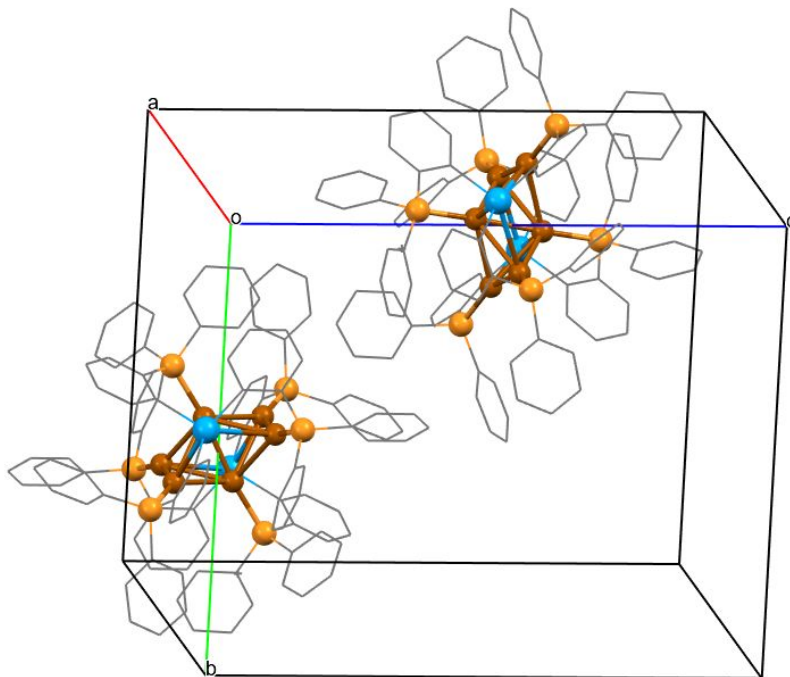


**Fig. 3** Crystal packing in the unit cell of the  $[\text{Au}_6(\text{PPh}_3)_2]^{2+}$  structure (Colour labels: brown/green = Au; orange = P; blue = Sb, grey = C; H atoms are not shown for clarity).

Looking closely at the crystal structure of  $[\text{Au}_6(\text{PPh}_3)_2]^{2+}$  cluster, we find that the unit cell comprises of two crystallographically independent halves of  $[\text{Au}_6(\text{SbP}_3)_2]^{2+}$  clusters (**Fig. 3**), where the two clusters are found at the sites of inversion symmetry and slightly differ in average bond lengths; hence, the average bond lengths of both  $[\text{Au}_6(\text{SbP}_3)_2]^{2+}$  cluster monomers are reported in **Table S3**. The average Au-Au bond distance in the crystal structure is  $2.760 \pm 0.048 \text{ \AA}$ , which is 4.2% shorter than bulk gold,  $2.88 \text{ \AA}$ , and is essentially identical to the experimental Au-Au average bond distance of  $2.759 \text{ \AA}$  in  $[\text{Au}_7(\text{dppp})_4](\text{BF}_4)_3$ ,<sup>18</sup> which also has a bitetrahedron gold core and a  $\text{S}^2\text{P}^2$  configuration from the superatom electron count of 4.<sup>40</sup> Further, the Au-Au bond distance in  $[\text{Au}_6(\text{SbP}_3)_2][\text{PF}_6]_2$  is found to be similar to the Au-Au bond distances reported for  $[\text{Au}_6(\text{PPh}_3)_6]^{2+}$  and  $[\text{Au}_6(\text{dppp})_4]^{2+}$  with average Au-Au bond distances of  $2.759 \text{ \AA}$  and  $2.783 \text{ \AA}$  respectively.<sup>19,20</sup> This finding is of quintessential importance as it is well-established that the bitetrahedral geometry is a result of strong Au-Au interaction in these clusters, which in turn, is determined by the optimum ligand architecture (or more specifically the cone-angle). Thus, it can be safely argued that our ligand  $\text{SbP}_3$  has an optimum-architecture to stabilize the bi-tetrahedral  $\text{Au}_6$  geometry. This also illustrates the importance of ligand design for exploring gold cluster chemistry.

The average Au-P bond distance in  $[\text{Au}_6(\text{SbP}_3)_2][\text{PF}_6]_2$  is ca. 2.3 Å, comparable to Au-P bond distances previously reported for other gold clusters.<sup>19,41</sup> The average Au-Sb bond distances were found to be  $3.095 \pm 0.137$  Å, where one of the Au-Sb bonds on each side of each cluster is ~10% longer than the other two bonds. These Au-Sb bond distances are much greater than the Au-Sb bond distance of  $2.48 \pm 0.02$  Å obtained for  $[\text{Au}_{13}(\text{SbPh}_3)_8\text{Cl}_4]^+$  cluster as well as the Au-Sb distance of  $2.549 \pm 0.027$  Å in  $\text{Au}_{18}(\text{S-Adm})_8(\text{SbPh}_3)_4\text{Br}_2$ .<sup>12,13</sup> This demonstrates that Au-Sb bond lengths, and thus the geometric aspects of gold clusters, can be tuned using novel stibine-based ligands. Further, even though a longer bond suggests a weaker interaction, the formation of a stable gold cluster indicates that the overall interaction between the metal centre and ligands are re-enforced via the synergistic effect of mixed ligands.

To obtain further insight into the geometric and optical properties of this cluster, theoretical calculations were performed as described in the Computational Details. At the BP86-D3/DZP level of theory, the Au-Au and Sb-C bonds are ~0.02 Å larger than the crystal structures as seen in **Table S3**. The average Au-Sb bond lengths are 0.017 Å shorter than the average distances in the two  $[\text{Au}_6(\text{SbP}_3)_2]^{2+}$  cluster monomers in the crystal structure, and the Au-P and P-C bonds remain essentially the same, with a variation of less than 0.009 Å. The bitetrahedron core of the cluster is essentially achiral, and the addition of the ligands makes the entire cluster chiral as shown by the theoretical circular dichroism spectrum in **Fig. S6**. The average bond distances in  $[\text{Au}_6(\text{PPh}_3)_6]^{2+}$  are almost the same compared to  $[\text{Au}_6(\text{SbP}_3)_2]^{2+}$  with Au – Au, Au – P, and P – C bond distances of  $2.774 \pm 0.045$  Å,  $2.307 \pm 0.009$  Å, and  $1.818 \pm 0.004$  Å, respectively.<sup>18</sup>

$[\text{Au}_6(\text{SbP}_3)_2]^{2+}$  and  $[\text{Au}_6(\text{PPh}_3)_6]^{2+}$  only have one occupied P molecular orbital, which breaks the spherical symmetry of the superatom model. This gives a large energetic gap between the P' HOMO and P' LUMO of 1.94 eV and 1.97 eV respectively for  $[\text{Au}_6(\text{SbP}_3)_2]^{2+}$  and  $[\text{Au}_6(\text{PPh}_3)_6]^{2+}$  at the BP86-D3/DZP level of theory. Further, there are no degeneracies between the HOMO and HOMO-1, as shown in the molecular orbital (MO) diagrams in **Fig. S7** and **S8**. (To compare between the ellipsoid and spherical basis, P' and D' refer to the elongated equivalents of the P and D superatomic orbitals.) Despite the incredibly similar Au-Au geometric structure in the  $\text{Au}_6$  clusters, as well as a similar atomic contribution in the HOMO, the p orbitals from Sb atoms directly mix into the frontier orbitals of  $[\text{Au}_6(\text{SbP}_3)_2]^{2+}$ . This causes smaller energetic gaps between the frontier orbitals.

The theoretical optical absorption spectrum of  $[\text{Au}_6(\text{SbP}_3)_2]^{2+}$  at the BP86-D3/DZP level of theory matches well with experiment with peaks at 3.30 eV (368 nm) and 2.81 eV (442 nm) (**Fig. 4(A)**); however, as a result of the Sb mixing, the vertical excitation energies are closer together, which forms more of a manifold rather than discrete electronic states, as seen in **Fig. 4(C)**. Investigation of the MOs involved in these transitions show charge transfer character where there is little to no overlap in electronic density between the occupied MOs, dominated by s and p atomic orbitals from the Au, P, and Sb atoms, and the virtual MOs, which primarily arise from carbon contributions in the aromatic groups (**Fig. S9** and **Fig. S10**). Exchange-correlation functionals at the generalized gradient approximation (GGA) level, such as BP86, do

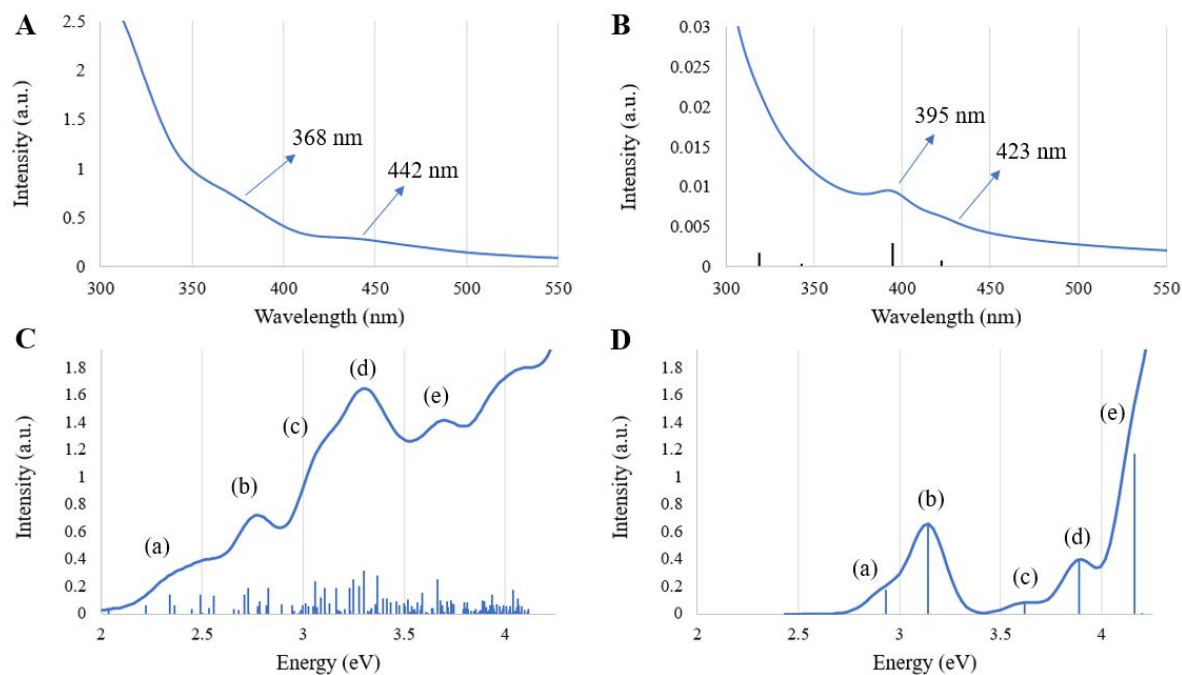


**Fig. 4:** Absorption spectrum of  $[\text{Au}_6(\text{SbP}_3)_2]^{2+}$ . (A) Experiment (B) LRCF-D3/DZP//BP86-D3/DZP spectrum in nm. (C) BP86-D3/DZP//BP86-D3/DZP in eV. (D) LRCF-D3/DZP//BP86-D3/DZP spectrum in eV.

not account for charge transfer;<sup>42</sup> therefore, to further distinguish the optical properties of this cluster, a long range corrected hybrid functional (LRCF) was used in a linear response calculation at the BP86-D3/DZP  $S_0$  geometry. The vertical excitation energies of the peaks with this functional, compared to BP86, can be seen in **Table S4**. The LRCF-D3/DZP//BP86-D3/DZP level of theory (**Fig. 4(B)**) shows good spectral similarity with experiment, and the dominant excitation can be seen at 395 nm (3.14 eV). Due to the long-range interactions, the vertical excitations show more discrete transitions than with BP86 as seen in the vertical excitation energies (**Fig. 4(D)**). It is important to note that despite the better energetic treatment, the long-range interactions overestimate the experimental energy, as well as the energetic gaps between orbitals; this overestimation, however, is a common artifact of this type of functional.<sup>43-45</sup> In this cluster, there is an intraband transition originating from the  $S_2$  state dominated by the HOMO  $\rightarrow$  LUMO+1 transition, and  $S_1$  state dominated by the HOMO  $\rightarrow$  LUMO transition at 2.93 eV. As an atomically precise gold cluster that is less than 2 nm, these gold core  $\rightarrow$  gold core transitions are expected to dominate the low energy optical peak(s), which is precisely what happens at this level of theory.

The second peak occurs at 3.14 eV and originates from the  $S_3$  state dominated by a HOMO  $\rightarrow$  LUMO+2 transition and an  $S_2$  state dominated by a HOMO  $\rightarrow$  LUMO+2. The molecular orbitals responsible for the transition of this peak can be seen in **Fig. 5**. Due to the geometric distortion in the core, the P' HOMO has large atomic orbital contributions from the sp orbitals on the gold atoms, but it is lengthened from the prolate geometric nature. This leads to an orbital that may better be described as a cluster  $\pi$  orbital rather than as an atomic p (or superatomic P) orbital. Furthermore, the slight mixing of p orbitals

from the Sb atoms in the L+2 MO pulls the electronic density away from the Au atoms, essentially flattening the once spherically symmetric four-lobed D orbital. This distortion in the D' orbital results in a lack of overlap of electronic density with the occupied orbital. As the Sb atoms are already mixing into  $[\text{Au}_6(\text{SbP}_3)_2]^{2+}$ , the stretched nature of the electronic density is exaggerated. The electronic density elongating due to the Sb atoms is not just an artifact seen in theoretical calculations, but it is also seen in experiment. The NMR analysis, for instance, showed a downfield shift of ca. 12 ppm in the phosphorous signal upon cluster formation. The molecular orbitals at the BP86-D3/DZP and LRCF-D3/DZP//BP86-D3/DZP level of theory in the first 12 frontier orbitals are displayed in **Fig. S11-Fig. S13**.

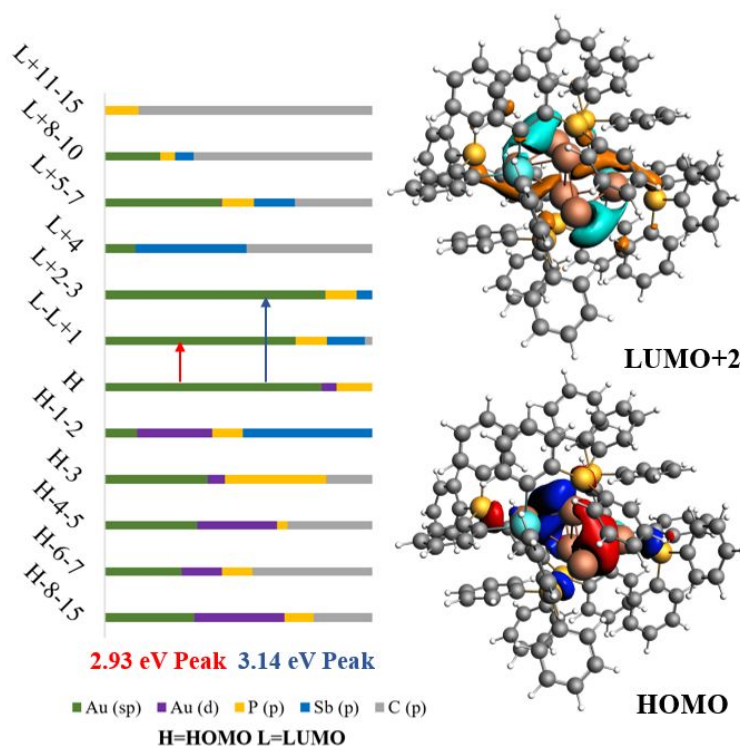


**Fig. 5:** Molecular orbital details at the LRCF-D3/DZP level of theory at the BP86-D3/DZP  $S_0$  geometry for  $[\text{Au}_6(\text{SbP}_3)_2]^{2+}$ . (A) Atomic orbital contributions to molecular orbitals and (B) Molecular orbitals responsible for the 3.14 eV peak.

The optical absorption spectra of  $[\text{Au}_6(\text{PPh}_3)_6]^{2+}$  at the BP86-D3/DZP level of theory is very different from that of  $[\text{Au}_6(\text{SbP}_3)_2]^{2+}$  despite the similar geometric structure and same amount of superatomic electrons as seen in **Fig. S14**. Of note, there is a much smaller energetic gaps between the frontier orbitals, which drastically changes the single orbital transitions in the theoretical absorption spectrum. Specifically,  $[\text{Au}_6(\text{SbP}_3)_2]^{2+}$  has a lot more mixing of single orbital transitions underneath the peaks, whereas  $[\text{Au}_6(\text{PPh}_3)_6]^{2+}$  has one dominant excitation in the low energy regime. Analyzing these clusters at the LRCF-D3/DZP//BP86-D3/DZP, they share more spectral similarities as  $[\text{Au}_6(\text{PPh}_3)_6]^{2+}$  also has an intraband transition originating from the  $S_2$  state dominated by the HOMO  $\rightarrow$  LUMO+1 transition, and  $S_1$  state dominated by the HOMO  $\rightarrow$  LUMO transition at 2.88 eV as well as a second peak that originates from the  $S_3$  state dominated by a HOMO  $\rightarrow$  LUMO+2 transition and an  $S_2$  state dominated by a HOMO  $\rightarrow$  LUMO+2

at 3.44 eV as seen in **Fig. S15**. Despite the similar electronic transitions, however, the electronic density of these transitions is very different between the two clusters as seen in **Fig. S16** and **Fig. S17**.

As already mentioned, apart from strong Au-Au interactions, the overall ligand-architecture determines the formation and stability of bi-tetrahedral Au<sub>6</sub> clusters. To verify the role of ligand structure, a new ligand SbP<sub>2</sub> was synthesized, and formation of Au clusters were attempted under similar synthetic conditions.<sup>15,25</sup> However, with SbP<sub>2</sub>, gold cluster formation was not observed, and the final product of the reactions were large brown-red gold nanoparticles. In a related study, Salorinne *et.al.* have already demonstrated that minimal changes in ligand structure can have significant effect on stability of gold-coordination clusters stabilized by a mixed ligand concept.<sup>46</sup> The ligand designed by them contained NHC-coordinating site as well as thiolate coordinating site. It was observed that the length of the “tether” connecting these two coordinating sites actually determines the stability of the resultant cluster. Our observation reinstates the same fact and the importance of effective design of ligands. The structure, synthetic details and <sup>1</sup>HNMR spectra of SbP<sub>2</sub> has been provided in the Supporting Information (**S1.4** and **Fig. S19**).

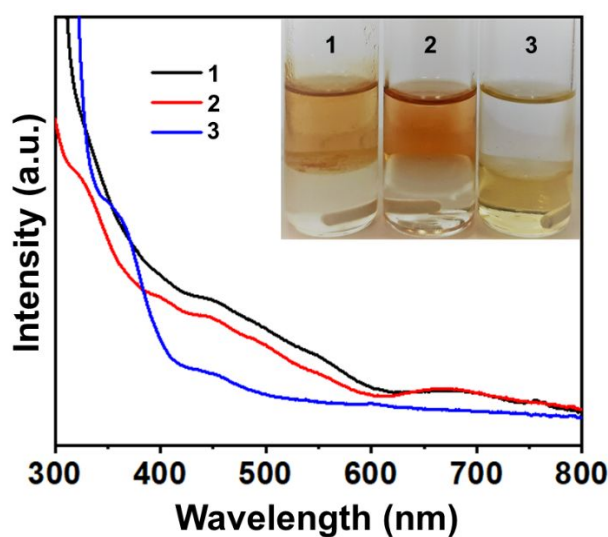


**Fig. 6:** UV-vis spectra of the products of the two-phase ligand exchange reaction in presence of excess glutathione (GSH) under aerobic conditions of (1) monodentate triphenylstibine-protected Au<sub>13</sub> clusters (black-trace); (2) monodentate triphenylphosphine-protected Au<sub>11</sub> clusters (red-trace), both of which convert to a water-soluble Au<sub>25</sub>(SG)<sub>18</sub> cluster within 30 minutes and 4 hours, respectively while (3) the multidentate ligand-protected [Au<sub>6</sub>(SbP<sub>3</sub>)<sub>2</sub>]<sup>2+</sup> clusters (blue-trace) are stable even after 6 hours illustrating its highly enhanced stability.

Despite the lack of spherically symmetric orbitals in the core, [Au<sub>6</sub>(SbP<sub>3</sub>)<sub>2</sub>][PF<sub>6</sub>]<sub>2</sub> shows remarkable thermal stability. At 70°C, the cluster shows little to no decomposition for 16 hours (**Fig. S18**). Further, the stability and reactivity of the [Au<sub>6</sub>(SbP<sub>3</sub>)<sub>2</sub>][PF<sub>6</sub>]<sub>2</sub> cluster was compared between monodentate stibine-protected Au<sub>13</sub> and phosphine-protected Au<sub>11</sub> clusters to study the effects of multidentate SbP<sub>3</sub> ligand coordination in the presence of excess glutathione (GSH) in a previously reported two-phase reaction.<sup>10,12</sup>

Unlike both the monodentate ligand-protected Au<sub>13</sub> and Au<sub>11</sub> clusters which convert to a water-soluble Au<sub>25</sub>(SG)<sub>18</sub> cluster with 8 superatomic electrons, it is observed that the [Au<sub>6</sub>(SbP<sub>3</sub>)<sub>2</sub>][PF<sub>6</sub>]<sub>2</sub> cluster does not react or decompose when treated with excess glutathione and remains intact in the organic phase (**Fig. 6**). This behaviour of the [Au<sub>6</sub>(SbP<sub>3</sub>)<sub>2</sub>][PF<sub>6</sub>]<sub>2</sub> cluster matches with that of the mixed stibine-thiolate Au<sub>18</sub>(S-Adm)<sub>8</sub>(SbPh<sub>3</sub>)<sub>4</sub>Br<sub>2</sub> cluster,<sup>13</sup> thereby validating the use of multidentate ligand platforms as a viable strategy to generate robust stibine-based metal clusters.

## Conclusion

In summary, a new gold cluster formulated as [Au<sub>6</sub>(SbP<sub>3</sub>)<sub>2</sub>][PF<sub>6</sub>]<sub>2</sub> stabilized by a multidentate ligand containing both stibine and phosphine moieties has been synthesized and structurally determined using single-crystal X-ray crystallography. This, to the best of our knowledge, is the first report of a gold cluster stabilized by synergistic stibine-phosphine coordination. This cluster demonstrates an edge-sharing bi-tetrahedral Au<sub>6</sub>-core, unlike the “core+exo” structures that are more common with multidentate ligands in literature.<sup>18,19</sup> The [Au<sub>6</sub>(SbP<sub>3</sub>)<sub>2</sub>][PF<sub>6</sub>]<sub>2</sub> cluster demonstrates excellent thermal stability. The chemical stability of this cluster in presence of excess thiol (glutathione) has also been compared to monodentate stibine- and phosphine-protected gold clusters. It is observed that despite the break of spherical symmetry, as determined from theoretical calculations, [Au<sub>6</sub>(SbP<sub>3</sub>)<sub>2</sub>][PF<sub>6</sub>]<sub>2</sub> shows no signs of decomposition in presence of excess thiol in sharp contrast to the control systems. In addition, no cluster formation is observed in presence of another mixed phosphine-stibine ligand (SbP<sub>2</sub>) under similar experimental conditions in which formation of [Au<sub>6</sub>(SbP<sub>3</sub>)<sub>2</sub>][PF<sub>6</sub>]<sub>2</sub> occurs. This demonstrates that the ligand SbP<sub>3</sub> has unique characteristics and structural attributes that change the optical properties of Au<sub>6</sub> clusters. These results are expected to spur the design of new multidentate ligands which, in turn, should lead to the development of robust clusters with *yet-unknown* properties.

## Acknowledgements

A.D thanks Southern Methodist University for start-up funds. S.H. and C.M.A. were supported by the National Science Foundation (CHE-1905048) of the United States. The computing for this work was performed on the Beocat Research Cluster at Kansas State University, which is funded in part by NSF grants CHE-1726332, CNS-1006860, EPS-1006860, and EPS-0919443.

## Conflict of Interest

The authors declare no conflict of interest.

## Corresponding Author Information

Dr. Anindita Das [Experiment]

Email: [aninditad@mail.smu.edu](mailto:aninditad@mail.smu.edu)

Dr. Christine M. Aikens [Theory]

Email: [cmaikens@ksu.edu](mailto:cmaikens@ksu.edu)

## Notes and references

- 1 R. Jin, C. Zeng, M. Zhou and Y. Chen, *Chem. Rev.*, 2016, **116**, 10346-10413.
- 2 I. Chakraborty and T. Pradeep, *Chem. Rev.*, 2017, **117**, 8208-8271.
- 3 M. Walter, J. Akola, O. Lopez-Acevedo, P. D. Jadzinsky, G. Calero, C. J. Ackerson, R. L. Whetten, H. Grönbeck and H. Häkkinen, *Proc. Natl. Acad. Sci.*, 2008, **105**, 9157-9162.
- 4 C. M. Aikens, *Acc. Chem. Res.*, 2018, **51**, 3065-3073.
- 5 N. A. Sakthivel and A. Dass, *Acc. Chem. Res.*, 2018, **51**, 1774-1783.
- 6 Q. Yao, T. Chen, X. Yuan and J. Xie, *Acc. Chem. Res.*, 2018, **51**, 1338-1348.
- 7 Y. Shichibu and K. Konishi, *Small*, 2010, **6**, 1216-1220.
- 8 S.-S. Zhang, L. Feng, R. D. Senanayake, C. M. Aikens, X.-P. Wang, Q.-Q. Zhao, C.-H. Tung and D. Sun, *Chem. Sci.*, 2018, **9**, 1251-1258.
- 9 Z. Lei, X. -K. Wan, S. -F. Yuan, Z. -J. Guan, Q. -M. Wang, *Acc. Chem. Res.*, 2018, **51**, 2465-2474.
- 10 L. C. McKenzie, T. O. Zaikova and J. E. Hutchison, *J. Am. Chem. Soc.*, 2014, **136**, 13426-13435.
- 11 X. Kang and M. Zhu, *Small* **2019**, *15* (43), 1902703.
- 12 Y.-Z. Li, R. Ganguly, K. Y. Hong, Y. Li, M. E. Tessensohn, R. Webster and W. K. Leong, *Chem. Sci.*, 2018, **9**, 8723-8730.
- 13 J. B. Patty, S. Havenridge, D. Tietje-Mckinney, M. A. Siegler, K. K. Singh, R. Hajy Hosseini, M. Ghabin, C. M. Aikens and A. Das, *J. Am. Chem. Soc.*, 2022, **144**, 478-484.
- 14 J. S. Jones and F. P. Gabbai, *Acc. Chem. Res.*, 2016, **49**, 857-867.
- 15 I.-S. Ke and F. P. Gabbai, *Inorg. Chem.*, 2013, **52**, 7145-7151.
- 16 X. Wan, Z. Lin and Q. M. Wang, *J. Am. Chem. Soc.* 2012, **134**, 14750-14752.
- 17 Q. F. Zhang, X. Chen and L. S. Wang, *Acc. Chem. Res.* 2018, **51**, 2159-2168.
- 18 Y. Shichibu, M. Zhang, Y. Kamei, and K. Konishi, *J. Am. Chem. Soc.*, 2014, **136**, 12892-12895.
- 19 J. W. A. Van der Velden, J. J. Bour, J. J. Steggerda, P. T. Beurskens, M. Roseboom, and J. H. Noordik, *Inorg. Chem.*, 1982, **21**, 12, 4321-4324.
- 20 C. E. Briant, K. P. Hall, D. M. P. Mingos and A. C. Wheeler, *J. Chem. Soc. Dalton Trans.*, 1986, 687-692.
- 21 M. Manassero, L. Naldini and M. Sansoni, *J. Chem. Soc. Chem. Comm.*, 1979, 385-386.
- 22 J. W. A. Van Der Velden, J. J. Bour, W. P. Bosman, J. H. Noordik, *Inorg. Chem.* 1983, **22**, 1913 - 1918.
- 23 J. W. A. van der Velden, J. J. Bour, B. F. Otterloo, W. P. Bosman, and J. H. Noordik, *J. Chem. Soc., Chem. Commun.*, 1981, 583-584.
- 24 S. Kenzler, M. Kotsch, A. Schnepf, *Eur. J. Inorg. Chem.* 2018, 3840-3848.
- 25 S. Bontemps, H. Gornitzka, G. Bouhadir, K. Miqueu and D. Bourissou, *Angew. Chem. Int. Ed.* 2006, **45**, 1611-1614.
- 26 Y. Shichibu, Y. Negishi, T. Tsukuda, and T. Teranishi *J. Am. Chem. Soc.*, 2005, **127**, 13464-13465.
- 27 G. te Velde, F.M. Bickelhaupt, E.J. Baerends, C. Fonseca Guerra, S.J.A. van Gisbergen, J.G. Snijders and T. Ziegler, *J. Comput. Chem.*, 2001, **22**, 931-967.
- 28 E. van Lenthe, A. Ehlers and E.-J. Baerends, *J. Chem. Phys.*, 1999, **110**, 8943-8953.
- 29 J.J. Goings, J.M. Kasper, F. Egidi, S. Sun and X. Li, *J. Chem. Phys.*, 2016, **145**, 104107.
- 30 J.P. Perdew, *Phys. Rev. B.*, 1986, **33**, 8822-8824.
- 31 A.D. Becke, *Phys. Rev. A.*, 1988, **38**, 3098-3100.
- 32 S. Grimme, S. Ehrlich and L. Goerigk, *J. Comput. Chem.*, 2011, **32**, 1456-1465.
- 33 E. Van Lenthe and E.J. Baerends, *J. Comput. Chem.*, 2003, **24**, 1142-1156.
- 34 R. Rüger, E. van Lenthe, T. Heine and L. Visscher, *J. Chem. Phys.*, 2016, **144**, 184103.
- 35 C. Bannwarth and S. Grimme, *Comput. Theor. Chem.*, 2014, **45**, 1040-1041.
- 36 M. Seth and T. Ziegler, *J. Chem. Theory. Comput.*, 2012, **8**, 901-907.
- 37 M.A. Tofanelli and C.J. Ackerson, *J. Am. Chem. Soc.*, 2012, **134**, 16937-16940.
- 38 M. Walter, J. Akola, O. Lopez-Acevedo, P. D. Jadzinsky, G. Calero, C. J. Ackerson, R. L. Whetten, H. Grönbeck and H. Häkkinen, *Proc. Natl. Acad. Sci.*, 2008, **105**, 9157-9162.
- 39 W. A. de Heer, *Rev. Mod. Phys.*, 1993, **65**, 3.
- 40 P. A Clayborne, O. Lopez-Acevedo, R. L. Whetten, H. Grönbeck and H. Häkkinen, *J. Chem. Phys.*, 2011, **135**, 094701.
- 41 L.-Y. Yao and V. W.-W. Yam, *J. Am. Chem. Soc.*, 2016, **138**, 15736-15742.
- 42 A. Dreuw, J. L. Weisman and M. Head-Gordon, *J. Chem. Phys.*, 2003, **119**, 2943.
- 43 R. Shinde, *ACS Omega*, 2016, **1**, 578-585.
- 44 B. M. Bold, M. Sokolov, S. Maity, M. Wanko, P. M. Dohmen, J. J. Kranz, U. Kleinekathöfer, S. Höfener and M. Elstner, *Phys. Chem. Chem. Phys.*, 2020, **22**, 10500-10518.
- 45 F. Rabilloud, *J. Phys. Chem. A.*, 2013, **117**, 4267-4278.
- 46 K. Salorinne, R. W. Man, P. A. Lummis, M. S. A. Hazer, S. Malola, J. C.-H. Yim, A. J. Veinot, W. Zhou, H. Häkkinen, M. Nambo and C. M. Crudden, *Chem. Commun.*, 2020, **56**, 6102-6105.